Example S-SAD phasing: requirements for data collection

Data collection:
Accurate
Redundant
Independent

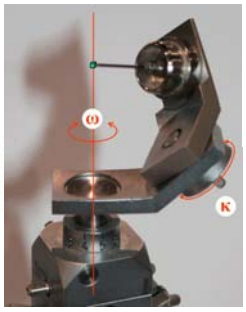

Scan	Scan type	ω	φ	2θ
1	180° ω	0°–180°	0°	0°
2	180° ω	30°–210°	0°	30°
3	180° ω	0°–180°	60°	0°
4	360° φ	0°	0°–360°	0°
5	180° ω	0°–180°	120°	0°
Anomalous redundancy calculated by strategy generator				~30
Total exposure time (60 s per image)				90 h

Table 8-8 Strategy for highly redundant data collection. The table entries contain the scan ranges and diffractometer angle settings for a highly redundant data collection strategy for the collection of anomalous data required for native sulfur single-wavelength anomalous diffraction (S-SAD) phasing for VTA1 (Laue symmetry 4/mmm).[79]

Example S-SAD phasing of a small protein

Anomalous data from native sulfur in disulfide bridges in VTA1, the small plant toxin in mistletoe.

Figure 10-28 Flow of S-SAD phasing. The basic steps of SAD phasing are neatly arranged in the *HKL2MAP* GUI. Analysis and preparation of anomalous difference data, search for the anomalous heavy atoms, and determination and extension of phases.

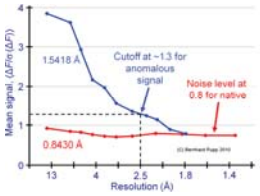

Figure 10-29 Empirical resolution cutoff for SAD phasing. The plot shows the signal level of the anomalous amplitude differences for the high-redundancy anomalous data collected at the Cu wavelength. In the case of the high-resolution data collected at the high energy wavelength of 0.8340 Å (red graph) practically no more 5 anomalous signal is measureable. An empirically well determined high resolution cutoff is around the point where the anomalous signal-to-noise ratio drops below 1.3.

Data cutoff is important for getting any solution.

Multisolution landscape with SHELXD

Figure 10-30 Effect of resolution truncation on heavy atom solution. Anomalous difference data are sensitive to noise, and need to be truncated at an optimal high resolution cutoff. A clear solution (right panel) is distinguished from a poor or wrong solution (left panel) by a discriminate solution landscape indicated by a clear drop in occupancy after a number of correct high occupancy sites were found. Note that a high number of trials may be necessary to find all sulfur sites with *SHELXD*.

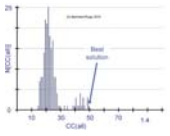

Sharp drop in occupancy after expected number of correct atoms is a sign of correct solution.

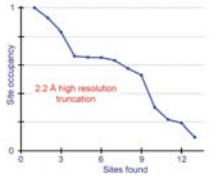

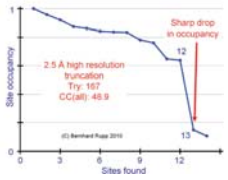

First maps determine substructure handedness

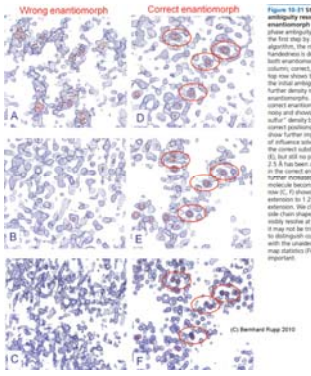

Figure 10-31 Stages of phase ambiguity resolution and enantiomorph selection. While the phase ambiguity is resolved internally in the first step by a low-density elimination algorithm, the metal substructure handedness is determined by trying both enantiomorphs (inverted, left column; correct, right column). The top row shows the maps at 2.5 Å after the initial ambiguity resolution (but no further density modification) for both enantiomorphs. Note the map from the correct enantiomorph (D) appears less noisy and shows the unresolved "super-sulfur" density blobs (red outline) in correct positions. The center row (B, E) show further improvement by sphere of influence solvent modification for the correct substructure enantiomorph (E), but still no phase extension beyond 2.5 Å has been attempted. The contrast in the correct enantiomorph map has further increased, and the outline of the molecule becomes distinct. The bottom row (C, F) shows the maps after phase extension to 1.25 Å in 20 cycles of phase extension. We clearly can distinguish side chain shapes and atoms begin to visibly resolve at this resolution (F). As it may not be trivial for the beginner to distinguish correct from poor maps with the unaided eye, attention to the map statistics (Figure 10-32) is vitally important.

The wrong substructure enantiomorph will not yield an interpretable map

Quantitative indicators of a 'good' map

Figure 10-32 Map contrast and final map correlation coefficient. The map contrast is a key indicator in the discrimination between correct and inverted heavy atom substructure enantiomorph (left panel). For the final map, the map correlation coefficient is an indicator for the resulting map quality. Given that the map correlation coefficient is approaching 0.95 over large parts of the map including the high resolution shells, we expect an exceptional experimental electron density map.

The map resulting from the correct substructure enantiomorph will show significantly better map contrast and map correlation coefficients.

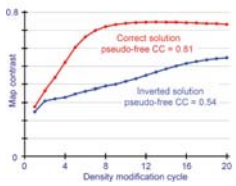

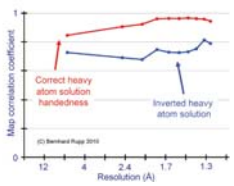

Visual appearance of a good map

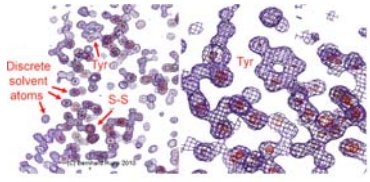

Clear contrast, good connectivity, and distinct protein features. This is an excellent experimental phase map. It does not have any model bias.

Figure 10-33 S-SAD experimental electron density of VTA1 at 1.25 Å resolution. As expected from the map correlation coefficient, which was above 0.9 for the high resolution reflections, we obtain an experimental map of outstanding quality. The delineation of protein and solvent is clear, and even discrete solvent molecules are visible. In the overview panel we also recognize high density of the S atoms in an S–S bridge, and from a helix viewed in cross section (compare Figure 12-28) protrudes a tyrosine residue with a nice hole in the aromatic ring. Because protein crystallographers tend to present holes in phenyl rings of experimentally phased maps with great pride, we share the detail view in the right panel.